

# COSMIC-RAY ACCELERATION AT ULTRARELATIVISTIC SHOCK WAVES: EFFECTS OF A “REALISTIC” MAGNETIC FIELD STRUCTURE

Jacek Niemiec

*Department of Physics and Astronomy, Iowa State University, Ames, IA 50011, USA  
and Institute of Nuclear Physics PAN, ul. Radzikowskiego 152, 31-342 Kraków, Poland*

niemiec@iastate.edu

and

Michał Ostrowski

*Astronomical Observatory, Jagiellonian University,  
ul. Orla 171, 30-244 Kraków, Poland*

## ABSTRACT

First-order Fermi acceleration processes at ultrarelativistic ( $\gamma \sim 5 - 30$ ) shock waves are studied with the method of Monte Carlo simulations. The accelerated particle spectra are derived by integrating the exact particle trajectories in a turbulent magnetic field near the shock. The magnetic field model upstream of the shock assumes finite-amplitude perturbations within a wide wavevector range and with a predefined wave power spectrum, imposed on the mean field component inclined at some angle to the shock normal. The downstream field structure is obtained as the compressed upstream field. We show that the main acceleration process at superluminal shocks is the particle compression at the shock. Formation of energetic spectral tails is possible in a limited energy range only for highly perturbed magnetic fields. Cutoffs in the spectra occur at low energies within the resonance energy range considered. These spectral features result from the anisotropic character of particle transport in the magnetic field downstream of the shock, where field compression produces effectively 2D perturbations. We also present results for parallel shocks. Because of the turbulent field compression at the shock, the acceleration process becomes inefficient for larger turbulence amplitudes, and features observed in oblique shocks are recovered in this case. For small-amplitude perturbations, particle spectra are formed

in the wide energy range, and modifications of the acceleration process due to the existence of long-wave perturbations are observed, as reported previously for mildly relativistic shocks. The critical turbulence amplitude required for efficient acceleration at parallel shocks decreases with increasing shock Lorentz factor  $\gamma$ . In both subluminal and superluminal shocks, an increase of  $\gamma$  leads to steeper spectra with lower cut-off energies. The spectra obtained for the “realistic” background conditions assumed in our simulations do not converge to the “universal” spectral index claimed in the literature. Thus the role of the first-order Fermi acceleration in astrophysical sources hosting relativistic shocks requires serious reanalysis.

*Subject headings:* acceleration of particles, cosmic rays, gamma rays: bursts, methods: numerical, relativity, shock waves

## 1. INTRODUCTION

At relativistic shock waves the bulk flow velocities are comparable to particle velocities. This leads to highly anisotropic particle distributions at the shock. Unlike the case of nonrelativistic shocks, acceleration processes are very sensitive to the background conditions, in particular to the structure of the perturbed (“turbulent”) magnetic field and the details of particle-wave interactions. These are, however, poorly known and modeling of the particle acceleration must rely on simplifying assumptions regarding particle scattering and transport. Here we consider the first-order Fermi acceleration processes, involving only the high-energy particles with gyroradii much greater than the thickness of the shock.

The first consistent semianalytic method to study the acceleration process at parallel relativistic shock was proposed by Kirk & Schneider (1987) and it was further extended to treat more general conditions at the shock by Heavens & Drury (1988). The method uses the stationary Fokker-Planck pitch-angle diffusion equation describing anisotropic particle distributions near the shock. Matching the upstream and downstream solutions of the diffusion equation at the shock yields both the power-law index of the resulting spectrum and the form of anisotropic particle angular distribution. The spectral indices for the phase space distribution function,  $\alpha$ , derived with this method for parallel relativistic shocks are different from the value of  $\alpha_{\text{NR}} = 4$  (or the equivalent *energy* spectral index  $\sigma_{\text{NR}} = \alpha_{\text{NR}} - 2 = 2$ ) obtained for strong nonrelativistic shocks (e.g., Drury 1983) and depend on the wave power spectrum of the magnetic field perturbations ( $\equiv$  the form of the pitch-angle diffusion coefficient). The same approach, augmented by the assumption of magnetic moment conservation for particles interacting with the shock, was used to study acceleration processes in oblique

subluminal shocks by Kirk & Heavens (1989). They proved that oblique shocks provide harder spectra than the parallel ones and the spectral index  $\alpha$  approaches 3 when the shock velocity along magnetic field lines is close to the speed of light. In the weakly perturbed conditions they assumed, the particle density upstream of the shock can be much larger than its downstream value (Ostrowski 1991), which results from the very effective multiple reflections of anisotropically distributed upstream particles from the compressed downstream magnetic field.

The validity of the semianalytic approximation is restricted to the case of a weakly perturbed magnetic field, where cross-field diffusion does not play a significant role. As discussed by Begelman & Kirk (1990), application of such conditions in perpendicular (superluminal) shocks does not allow for the diffusive acceleration process, since particles are not able to cross the shock front repeatedly. Instead, the shock-drift acceleration process, involving a single transmission of upstream cosmic ray particles through the shock (Webb, Axford, & Terasawa 1983; Drury 1983) shapes the particle spectrum in superluminal shocks. As a result, the distribution of accelerated particles downstream of the shock is the upstream particle distribution compressed and shifted to higher energies. Because of particle angular distribution anisotropy, the mean energy gain of particles transmitted through the shock is larger than the one expected from the adiabatic compression.

Efficient particle cross-field scattering can be accomplished if finite-amplitude MHD waves occur near the shock. They may preexist in the turbulent ambient medium upstream of the shock, but they can be also generated by the accelerated particles themselves (as in nonrelativistic shocks, see, e.g., Drury 1983; Lucek & Bell 2000). In such conditions, investigations of the acceleration processes must rely on numerical methods. A role of finite-amplitude magnetic field perturbations in forming particle spectra at relativistic shocks was investigated by a number of authors using Monte Carlo particle simulations (e.g., Ellison et al. 1990; Ostrowski 1991, 1993; Ballard & Heavens 1992; Naito & Takahara 1995; Bednarz & Ostrowski 1996, 1998). A direct dependence of the (power-law) particle spectra on the assumed conditions near the shock was proved. For different mean magnetic field inclinations with respect to the shock normal and different amplitudes of perturbations, the spectra can be either steep or flat, and variations of the particle spectral index can be non-monotonic at the transition from weakly perturbed conditions to highly nonlinear magnetic field perturbations (Ostrowski 1991, 1993). For highly turbulent magnetic fields, power-law spectra can be also formed at superluminal shocks. They are, however, very steep for mildly perturbed conditions.

The power spectra of realistic perturbed magnetic fields can differ by such parameters as the amplitude and the spectral index for the considered power-law distributions, but

also the wavevector range of the distribution and its possible anisotropy or nonuniformity. The first step to study such realistic features was presented for mildly relativistic shocks in a recent paper (Niemiec & Ostrowski 2004),<sup>1</sup> where we considered the power-law wave spectra upstream of the shock within a relatively wide range of wavevectors, with only static perturbations involved. The perturbations are imposed on the mean field component, inclined at a given angle to the shock normal. The downstream magnetic field structure was derived by assuming a simple shock compression of the upstream field, thus preserving the continuity of the perturbed magnetic field across the shock. By choosing different amplitudes and spectral indices of the turbulence and different mean field inclinations, we were able to study the acceleration processes in a variety of background conditions, including both sub- and superluminal shocks with varying amount of background perturbations. The model allowed us also to investigate the role — in the shock acceleration — of short, resonance and long waves at different particle energies, to better understand the microphysics of the acceleration processes. The study showed that the particle spectra generally diverge from a simple power law; the exact shape of the spectrum depends on both the amplitude and the wave power spectrum of the magnetic field perturbations. We reported and discussed such features as spectrum hardening before the cutoff at high particle energies in oblique subluminal shocks, and the steepening of the spectrum and the cutoff formation in the resonance energy range in superluminal shocks. In the latter case, the role of the long-wave magnetic field perturbations proved to be critical for the generation of the power-law spectral tails. For parallel shocks, we showed that the presence of finite-amplitude magnetic field perturbations leads to the formation of locally oblique field configurations at the shock and the respective magnetic field compressions. This implies a qualitative modification of the particle acceleration process by introducing some features present in oblique shocks. As a result, nonmonotonic variations of the particle spectral index with the turbulence amplitude were observed.

In the present paper we slightly modify the above approach to study shocks with larger Lorentz factors  $\gamma \gg 1$ . Besides several detailed results, we report significant difficulties to

---

<sup>1</sup>The two earlier papers by Ballard & Heavens (1992) and Ostrowski (1993), which incorporated some “realistic” features of the magnetic field near the shock, had to apply a very simplified modeling of the turbulent field structure (see Niemiec & Ostrowski (2004); here we want to correct some inaccuracies concerning the simulations of Ballard & Heavens (1992), which appeared in our paper: rather than having unrelated upstream and downstream turbulent fields, their magnetic fields were consistently transformed from upstream to downstream frame at the shock boundary; secondly, the same turbulent field was used throughout the integration of particle trajectories — there was no selection of a new turbulent field at each particle shock crossing).

form the wide-energy range power-law particle spectral tails in quasi-perpendicular shocks.<sup>2</sup> In most cases, including highly perturbed conditions at the shock, an energy cutoff appears in the particle spectrum within the considered resonance energy range for particle-wave interactions. Moreover, even for parallel shocks with the studied magnetic field structures, we do not observe spectral index convergence to the “universal” value discovered by Bednarz & Ostrowski (1998) and Gallant & Achterberg (1999) (see also discussion by Ostrowski & Bednarz 2002). These results are important in a wide context of interpreting the observational data on astrophysical sources involving highly relativistic plasma flows/shocks, such as active galactic nuclei, micro-quasars, gamma-ray bursts, as well as for the ultra-high-energy cosmic ray production problem. In a forthcoming paper we plan to extend the present analysis to situations including the generation of short-wave turbulence at the shock. Preliminary results of this work are presented in Niemiec (2005).

In what follows,  $c$  is the speed of light. All calculations are performed in the respective local plasma (upstream or downstream) rest frames. The upstream (downstream) quantities are labeled with the index ‘1’ (‘2’). We consider ultrarelativistic particles with  $p = E$ . In units we use in our simulations, a particle of an unit energy moving in an uniform mean upstream magnetic field  $B_{0,1}$ , has the unit maximum (for  $p_{\perp} = E$ ) gyroradius  $r_g(E = 1) = 1$  and the respective resonance wavevector  $k_{res}(E = 1) = 2\pi$ .

## 2. SIMULATIONS

The Monte Carlo approach we use here has been described in detail in Niemiec & Ostrowski (2004). Below we sketch the most important features of the method and discuss the modifications introduced in the present paper.

We consider a planar relativistic shock wave propagating with velocity  $u_1$  (Lorentz factor  $\gamma_1$ ) with respect to the magnetized upstream plasma. The upstream magnetic field is assumed to consist of the uniform component  $\mathbf{B}_{0,1}$ , inclined at some angle  $\psi_1$  to the shock normal, and finite-amplitude perturbations imposed upon it. The irregular component has either a flat ( $F(k) \sim k^{-1}$ ) or a Kolmogorov ( $F(k) \sim k^{-5/3}$ ) wave power spectrum in a wide wavevector range ( $k_{min}, k_{max}$ ). The downstream field structure, together with the downstream flow velocity  $u_2$ , are obtained from hydrodynamic shock jump conditions derived for the cold electron-proton plasma upstream of the shock. We use approximate formulae derived by Heavens & Drury (1988) to calculate the shock rest frame compression ratio

---

<sup>2</sup>One should note that nearly all magnetic field configurations in ultrarelativistic shocks lead to the perpendicular (superluminal) shock structure.

$R = u_1/u_2$  ( $R = 3$  for  $\gamma_1 \rightarrow \infty$ ). The acceleration process is studied by following exact particle trajectories in the perturbed magnetic field near the shock, without a simplifying hybrid approach used by Niemiec & Ostrowski (2004). Because the irregular field component is assumed to be static in the upstream and downstream plasma rest frames, the second-order Fermi acceleration is excluded from our considerations. Radiative (and other) energy losses are also neglected in this modeling.

## 2.1. Perturbed Magnetic Field Structure

The “turbulent” ( $\equiv$  perturbed) magnetic field component upstream of the shock is modeled as a superposition of static sinusoidal waves of finite amplitude. In the magnetic field related *primed* coordinate system,<sup>3</sup> they take the form:

$$\delta B_{x'} = \sum_{l=1}^{294} \delta B_{x'l} \sin(k_{x'y'}^l y' + k_{x'z'}^l z'), \quad (1)$$

where  $(k_{x'y'}^l)^2 + (k_{x'z'}^l)^2 = (k_{x'}^l)^2$  (see below), and analogously for  $\delta B_{y'}$  and  $\delta B_{z'}$  components. Such a form of  $\delta \mathbf{B}$  for 3D turbulence (see Giacalone & Jokipii 1994; Michałek & Ostrowski 1997) ensures that  $\nabla \cdot \mathbf{B} = 0$ . The index  $l$  enumerates the logarithmic wavevector range from which the wavevectors  $k_i^l$  ( $i = x', y', z'$ ) are randomly drawn. The components  $k_{x'y'}^l, k_{x'z'}^l$  of the wavevectors  $k_{x'}^l$  are selected by choosing a random phase angle  $\phi_{x'}^l$ , so that  $k_{x'y'}^l = k_{x'}^l \cos \phi_{x'}^l$  and  $k_{x'z'}^l = k_{x'}^l \sin \phi_{x'}^l$ , and analogously for other components. The wavevectors span the range  $(k_{min}, k_{max})$ , where  $k_{min} = 0.0001$  and  $k_{max} = 10$ , and particle energies are formally related to these values by the resonance condition  $k_{res} = 2\pi/r_g(E)$ .

The respective wave amplitudes  $\delta B_{il}$  are selected at random, subject to the constraint  $\delta B_l^2 = \sum_i \delta B_{il}^2$ , where the amplitudes  $\delta B_l$  are chosen to reproduce the assumed turbulence power spectrum. In the wavevector range considered, it can be written as

$$\delta B_l(k) = \delta B_l(k_{min}) \left( \frac{k}{k_{min}} \right)^{(1-q)/2}, \quad (2)$$

where  $q$  is the spectral index:  $q = 1$  corresponds to the flat spectrum and  $q = 5/3$  to the Kolmogorov one. The constant  $\delta B_l(k_{min})$  is scaled to match the model parameter  $\delta B/B_{0,1}$

---

<sup>3</sup>In the upstream plasma rest frame the  $x$ -axis of the (unprimed) Cartesian coordinate system  $(x, y, z)$  is perpendicular to the shock surface. The shock wave moves in the negative  $x$ -direction and the regular magnetic field  $\mathbf{B}_{0,1}$  lies in the  $x - y$  plane. The primed system  $(x', y', z')$  is obtained from the unprimed upstream one by its rotation about the  $z$ -axis by an angle  $\psi_1$ , so that the  $x'$ -axis is directed along  $\mathbf{B}_{0,1}$ .

defined upstream of the shock, where  $\delta B \equiv [\sum_l \delta B_l^2]^{1/2}$  (or using the turbulence power spectrum  $F(k)$ ,  $\delta B^2 = \int F(k)dk$ ).

The downstream magnetic field structure is obtained as the compressed upstream field. According to the jump conditions at the shock (e.g., Heavens & Drury 1988; Kirk & Duffy 1999), only field components perpendicular to the shock normal are compressed, and the relativistic compression factor  $r = R\gamma_1/\gamma_2$  (where  $\gamma_i = 1/\sqrt{1-u_i^2}$  ( $i = 1, 2$ )) gives the compression ratio between the two plasma rest frames. One should note that in our approach the magnetic field lines are continuous across the shock. This allows one to study upstream–downstream correlations in particle motion introduced by the field structure, for different levels of turbulence, and to study the influence of this factor in forming particle spectra.

Although the Kolmogorov wave power spectrum considered in our modeling seems to properly describe magnetic field turbulence in a number of real astrophysical situations (see, e.g., the discussion in Niemiec & Ostrowski 2004), the actual field structure near the shock front can be far more complex. Nonlinear interactions between accelerated particles and the background plasma initiate the generation of MHD turbulence by plasma instabilities. Additionally, wave damping processes as well as nonlinear wave interactions influence the final turbulence spectrum. No currently used numerical approach allows one to study these processes in full, with involved nonlinearities and particle acceleration from thermal energies up to high-energy cosmic rays. Therefore, we limit our considerations to the test particle approach in the assumed background conditions. It restricts the validity of the study to the I-order Fermi acceleration process and particles with energies much higher than the “thermal” energies of the downstream plasma.

In the present simulations we assume that the shock front instabilities do not produce any additional fluctuations of the magnetic field. However, theoretical considerations (Medvedev & Loeb 1999) and numerical studies (e.g., Silva et al. 2003; Nishikawa et al. 2003; Frederiksen et al. 2004) suggest that additional strong, small-scale field components are generated downstream of the shock due to the relativistic filamentation instability. The effects of these small-scale perturbations will be investigated in our forthcoming paper.

## 2.2. Simulation Method and Particle Injection

The particle equations of motion are integrated in the local (upstream or downstream) plasma rest frame, where the electric field vanishes. The simulation run is divided into cycles. At the beginning of each cycle,  $N$  particles (usually  $N = 100$ ) are located at the shock front and Lorentz-transformed into the upstream plasma rest frame. The trajectory

of each particle is then followed until it crosses the shock surface, at which point the Lorentz transformation to the downstream plasma rest frame is performed. At this side of the shock a free escape boundary is located “far downstream” from the shock at  $x_{max}(E) = X_{max} \bar{r}_{g,2}(E_2)$  behind it (note that  $\bar{r}_{g,2}(E_2)$  is the particle gyroradius in the average downstream magnetic field). The selected value of the coefficient  $X_{max} \in (5, 100)$  depends on the chosen simulation parameters, and it is specified using numerical tests separately for each shock configuration. This ensures that the results are not influenced by  $X_{max}$ . In the conditions considered by us, very few particles are able to travel/diffuse from such distance back to the shock. A particle trajectory downstream of the shock is integrated until it crosses this escape boundary or reaches the shock front. After performing this procedure for all  $N$  particles, a simulation cycle is finished. Then the trajectory splitting procedure is applied, which replaces all escaped particles with the ones still active in the acceleration process, with the respective partition of particle statistical weights. In this way particle spectra are derived with approximately the same accuracy in a wide energy range (for details see Niemiec & Ostrowski 2004). The analogous subsequent cycles are repeated until either more than 90% of particles escape through the downstream boundary in an individual simulation cycle, or all particles reach the assumed upper energy limit  $E_{max,2}$  (given in the downstream rest frame), or the lower limit for the particle weight  $w$  is reached. The lower limit for  $w$  is usually set to  $10^{-6}$  of the initial weight  $w_0$ . The final spectra and angular distributions are averaged over several (10 - 50) simulation runs, each with statistically different sets of  $N$  particles and different realizations of the perturbed magnetic field.

At the beginning of a simulation run the particles are injected at the shock front with uniform angular distribution within the range of  $\cos \theta_2 \in (-1, -u_2)$  in the downstream plasma rest frame ( $\theta$  is the angle between the particle momentum and the shock normal), so that their momentum vectors in the upstream rest frame are in the cone around the shock normal with the opening angle  $\theta_c$  ( $\sin \theta_c = 1/\gamma_1$ ). They are monoenergetic in the downstream rest frame, and the injection energy  $E_i = E_{0,2} = 0.1$  is such that particle resonance wavevectors  $k_{res}(E_{0,2}) \gg k_{max}$ . Such initial conditions correspond roughly to the particle injection from the thermal plasma. For ultrarelativistic shocks considered here, the majority of the injected particles escape far downstream in the first simulation cycle. In order to improve the statistical accuracy of the spectra, we continue injecting particles in the first cycle until  $N$  of those which — after transmission downstream — succeed in reaching the shock front again are selected. These particles are used in a given simulation run and have the same initial weights  $w_0$ .



### 2.3. Derivation of Particle Trajectories

In the previous paper we developed a hybrid approach for modeling the motion of high-energy particles in the turbulent field including short MHD waves. It involves the exact integration of particle orbits in the perturbed field including long and resonance waves only, and the short-wave ( $\lambda_s \ll r_g$ ) influence on the trajectory is reproduced with a small-amplitude pitch-angle scattering term. A need for such approach arose due to excessive computation time required to derive exact trajectories in the magnetic field with short-wave perturbations. This limitation becomes less severe for ultrarelativistic shock acceleration studies because for the high- $\gamma$  shocks both upstream and downstream residence times are shorter than in the case of the previously investigated mildly relativistic shocks, and for a particle of a given energy these times decrease with  $\gamma$ . Thus, in the present paper we *do not* use the hybrid approach, and calculate particle orbits directly by integrating their equations of motion in the considered perturbed magnetic field near the shock.

In the computations we use the Runge-Kutta 5-th order method with the adaptive step size control (routine RKQS in: Press et al. 1992) for accurate derivation of particle trajectories in non-uniform magnetic field with the optimized simulation time. The accuracy imposed in our simulations (controlled by the truncation error set to be less than  $10^{-7}$ ) ensures that the integration time step is much smaller than the residence time upstream and downstream of the shock.<sup>4</sup> We checked by numerical tests, that the computed particle orbits are stable over more than the mean upstream and downstream residence time and the derived trajectories are reversible in time over their entire path. This proves that the numerical noise is maintained at the very low level, which is independently demonstrated by the accompanied diffusion coefficients derivations (see Appendix).

## 3. RESULTS

In the present work we use Monte Carlo simulations to study the role of the realistic magnetic field features on the first-order Fermi acceleration processes at ultrarelativistic shocks in the test particle approach. As pointed out by Begelman & Kirk (1990), most (essentially all) magnetic field configurations in the case of ultrarelativistic shocks lead to superluminal conditions for the acceleration process. However, our study includes the case of highly

---

<sup>4</sup>This requirement limits the use of the hybrid method for ultrarelativistic shocks. The trajectory perturbations due to the short waves with  $\lambda_s \ll r_g$  introduce diffusive modifications of particle trajectories on time scales much longer than  $\tau_s \equiv \lambda_s/c$ . When the residence time upstream or downstream of a high- $\gamma$  shock becomes comparable to  $\tau_s$  the hybrid method involving a diffusive term cannot be used.

perturbed magnetic fields. Results of the modeling for superluminal shocks are presented in §3.1. The structure of the compressed downstream magnetic field renders particle acceleration inefficient at such shocks — even in conditions of highly perturbed magnetic fields the particle spectra do not extend to very high energies, exhibiting cutoffs within the resonant range for particle-wave interactions. Parallel high- $\gamma$  shock configurations are studied in §3.2. We find that for larger amplitudes of the magnetic field perturbations, the spectral features similar to those observed in oblique shocks occur because of the effects of the magnetic field compression downstream of the shock. Only in the case of weakly perturbed fields, the flat power-law parts appear in the spectra due to the presence of long-wave perturbations.

Accelerated particle spectra formed at oblique superluminal shocks are presented in Figures 1 and 2, and the spectra derived for parallel shock waves in Figures 4 and 5. The background conditions for the respective spectra are indicated in the figures. The spectra have been calculated for different upstream magnetic field perturbation amplitudes  $\delta B/B_{0,1}$ . Some of the energetic particle spectral tails have a power-law form for the conditions considered, and in these cases linear fits to the power-law parts of the spectra are presented with the values of the (phase-space) spectral index  $\alpha$  given in the figures. Particles in the energy range indicated by arrows above the energy axis can interact with the magnetic field inhomogeneities with the resonant condition  $k_{res} \equiv 2\pi/r_g$  satisfied, where  $k_{min} \lesssim k_{res} \lesssim k_{max}$ . These limits are not precise, they are calculated for the upstream magnetic field strength  $B_{0,1} = 1$  and particle transverse momenta  $p_{\perp} = p$ . Note that the particle energies considered in the simulations can be approximately scaled to various conditions met in astrophysical shocks by the respective identifications of  $B_{0,1}$ ,  $\psi_1$ ,  $\delta B$ ,  $k_{min}$  and  $k_{max}$ .

### 3.1. Superluminal Shock Waves

The characteristic features of particle acceleration processes at oblique superluminal high- $\gamma$  shocks are illustrated in Figures 1 and 2.<sup>5</sup> All injected particles are initially accelerated in a phase of “superadiabatic” compression at the shock. Then, only a small fraction of these particles is further accelerated in the first-order Fermi process forming an energetic tail in the energy spectrum. The tail shape and its extension to high energies strongly depend on the magnetic field turbulence spectrum. For the same power of magnetic field perturbations, the existence and extension of the tails depends on how much wave energy is

---

<sup>5</sup>The results presented in Figure 1 for shocks with  $\gamma_1 = 5$  correspond to those obtained with the previously used hybrid method for particle trajectory calculations (see Fig. 9 in Niemiec & Ostrowski 2004) and proves the validity of this approximate approach.

contained in long-wave perturbations. For the flat wave power spectrum (with the spectral index  $q = 1$ ; Fig. 1a) the tails are steep and the resulting spectra of accelerated particles do not differ significantly from the pure compressed ones formed without any turbulence. For the high-amplitude Kolmogorov turbulence, with most power in long waves ( $q = 5/3$ ; Fig. 1b), much flatter high-energy tails are formed, which contain a substantial part of the accelerated particles energy density. These tails diverge from the power-law form by exhibiting a continuous steepening. For both types of wave spectra the cutoffs appear within the resonance energy range. To be noted from Figure 2 is that the cutoff energy decreases with growing shock Lorentz factor.

To understand these spectral features one has to consider the influence of the turbulence characteristics at energetic particle trajectories near the shock (see, e.g., Begelman & Kirk 1990; Ostrowski 1991, 1993; Bednarz & Ostrowski 1996; Niemiec & Ostrowski 2004). For the superluminal shock parameters considered here, with the projected velocity  $u_{B,1} \equiv u_1 / \cos \psi_1 \approx 1.4c$  in each case, a low amplitude of magnetic field perturbations leads to the accelerated particle spectrum being just the anisotropically compressed upstream injected distribution. In our approach, with approximately monoenergetic particle injection, this process can be seen in Figures 1 and 2 as a step-like spectral component at low energies. To enable the formation of a power-law tail at higher energies, some downstream particles must succeed in being transported back to the shock for continued energization after the initial compression phase. There are two features of the perturbed magnetic field which can provide a backward transport. Either the resonant waves with a substantial amplitude are present, which enable particle cross-field diffusion backward to the mean plasma flow, or long-wave perturbations form locally subluminal field configurations near the shock and some particles propagating in these regions succeed in reaching the shock again.

To better understand how these two factors can influence the acceleration process let us analyze them separately. To enable efficient cross-field diffusion behind the shock, large-amplitude three-dimensional resonant MHD perturbations (see, e.g., Giacalone & Jokipii 1994; Michałek & Ostrowski 1997; Jones et al. 1998) must be present. In the case of relativistic shock waves, the shock moves in the downstream plasma rest frame with velocity  $u_2 \approx c/3$  and the cross-field diffusion must approach its upper limit — the Bohm diffusion efficiency — in order to allow a sufficient fraction of downstream particles to remain continuously active in the energization process. This can be achieved in a relatively easy way by applying simplified turbulence modeling similar to those proposed in Ostrowski (1991), Ellison et al. (1990) or Bednarz & Ostrowski (1996, 1998), where by selecting specific parameters for small-amplitude particle pitch-angle scattering one allows for conditions with nearly isotropic particle diffusion, or the modeling of Ostrowski (1993), where upstream sinusoidal field perturbations are selected from the narrow, approximately resonance wavevector range

at all particle energies. Studies involving finite wavevector range turbulence spectra, like the ones considered in Niemiec & Ostrowski (2004) and in the present paper, show a substantial difficulty in generating the downstream field perturbations that allow for efficient cross-field diffusion.

The presence of long-wave ( $\lambda \gg r_g$ ) magnetic field perturbations of substantial amplitude changes the local shock conditions for particle acceleration. In superluminal shocks they form finite intermittent volumes near the shock with varying magnetic field obliquities, including the subluminal ones, where the acceleration process can proceed more easily and in some cases particle reflections from the shock can occur (see Niemiec & Ostrowski (2004) for the discussion of these effects in mildly relativistic shocks). However, for the in-average-perpendicular field configuration such subluminal regions are advected with the plasma flow and replaced by successive regions with possibly superluminal conditions, thus removing (advecting downstream) accelerated particles from the shock. Only the cross-field diffusion processes can redistribute some particles to new subluminal field configurations to extend the spectrum to higher energies. The injected particles that enter the acceleration process under superluminal local conditions do not reach energies much higher than possible with the initial compression only.

In the case of the flat wave power spectra (Fig. 1*a*) and highly perturbed conditions ( $\delta B/B_{0,1} = 1.0$  or  $3.0$  upstream of the shock) the amplitudes of resonant magnetic field perturbations are small upstream, and nonlinear downstream of the shock. However, the downstream compressed turbulence is strongly anisotropic, with most power in the magnetic field components parallel to the shock front,<sup>6</sup> which results in decreased particle diffusion efficiency along the shock normal (see Appendix). These downstream conditions are essentially independent of the initial particle energy, and the particle spectra for  $E_i = 0.1, 1$  and  $10$ , and for  $\delta B/B_{0,1} = 1.0$  in Fig. 1*a* have the same shape with the compressed step-like parts followed by the cutoff tails. At each upstream–downstream–upstream cycle most of the particles finish the cycle being advected far downstream from the shock, and only a few privileged ones meet suitable local magnetic field configurations that enable further energization. Thus the observed decrease in the cutoff tail inclination with particle energy, until a final sharp cutoff, results from this “subjective” selection of particles which can continue the acceleration and substitute the escaping ones in the successive simulation cycles. Such a tail is absent in the weakly perturbed case ( $\delta B/B_{0,1} = 0.3$ ), and the tails do not differ substantially between our mildly ( $\delta B/B_{0,1} = 1.0$ ) and highly perturbed ( $\delta B/B_{0,1} = 3.0$ ) cases.

---

<sup>6</sup>This structure should relax to more isotropic 3D one further downstream, but this relaxation process cannot be analyzed within the present approach.

In cases involving the Kolmogorov wave power spectrum (Fig. 1b), the physical situation is substantially modified. Here the acceleration process after particle injection proceeds through the “superadiabatic” shock compression phase, followed by the energetic spectral tail formation at the ensemble of shock conditions involving different local magnetic field inclinations, due to high amplitude of the long waves. The local regions with subluminal configurations are gradually advected downstream of the shock leading to steepening of the spectrum and a cutoff formation at  $E_{cut} \sim 10^4 E_0$ , independent of the particle injection energy, as exemplified by the spectra for  $E_i = 0.1, 1, 10$  and  $100$ , and for  $\delta B/B_{0,1} = 1.0$  in Fig. 1b. The cutoff energy is much below the resonance energy for the longest upstream waves ( $\sim 10^6 E_0$ ). It is difficult to judge which changing background factor dominates in determining  $E_{cut}$ : the lack of large extended regions of subluminal conditions near the shock for high-energy particles, or the decreasing efficiency of diffusion along the local mean magnetic field due to compressed medium-amplitude waves perturbing the downstream particle trajectories.

In Figure 2, one can observe a drastic reduction of the spectral tail and an accompanying decrease of  $E_{cut}$  with increasing shock Lorentz factor. At large  $\gamma_1$  the shock propagation velocity in the downstream plasma rest frame is essentially constant,  $u_2 \approx c/3$ . However, increasing  $\gamma_1$  leads to a decreasing normal diffusion downstream of the shock,<sup>7</sup> and that is the most important cause of decreasing of  $E_{cut}$ . An additional factor responsible for the observed changes of  $E_{cut}$  is a weaker particle scattering upstream of the shock for growing  $u_1 \rightarrow c$ , due to the shorter particle residence time before recrossing the shock downstream.

Figure 3 shows particle angular distributions for the superluminal shocks propagating in a mildly perturbed ( $\delta B/B_{0,1} = 1.0$ ) magnetic field. The distributions are calculated for particles forming energetic tails in the spectra shown in Figures 1 and 2. The differences in the angular distributions for  $\gamma_1 = 5$  and the Kolmogorov (*solid line*) and the flat (*dotted line*) turbulence illustrate the variation of the physical conditions for particle acceleration discussed above for both types of the perturbed magnetic field power spectra. In particular, the effects of long-wave perturbations for  $q = 5/3$ , which enable a larger fraction of particles to cross the shock back into the upstream region are apparent. The results for the Kolmogorov turbulence and for  $\gamma_1 = 10$  (*dashed line*) and  $\gamma_1 = 5$  show the effects of the increasing shock Lorentz factor on the angular distributions at the shock.

---

<sup>7</sup>For the cases shown in Fig. 2, the shock compression factor  $r = R\gamma_1/\gamma_2$  is 15.8, 29.5 and 86.4 for  $\gamma_1 = 5, 10$  and  $30$ , respectively.

### 3.2. Parallel High- $\gamma$ Shocks

The effects of downstream magnetic field compression observed in particle spectra formed at oblique shocks are also found in parallel ultrarelativistic shocks, where the considered high-amplitude turbulence is subject to compression. Accelerated particle spectra for parallel shocks with  $\gamma_1 = 10$  and 30 are shown in Figures 4 and 5, respectively, for different amplitudes and power spectra of the magnetic field perturbations. For small perturbation amplitudes, very flat spectra ( $\alpha < 4.0$ ), characteristic for oblique subluminal shocks, are generated. This is due to locally oblique magnetic field configurations formed by the long-wave perturbations at the shock front, and the respective field compressions downstream of the shock. The power-law parts of the spectra are followed by the cutoffs at high particle energies. The acceleration processes become less efficient for larger turbulence amplitudes. In these cases the acceleration mechanism resembles that acting at superluminal shocks: particle compression at the shock forms a step-like low-energy component of the spectrum, followed by the steeper (for the flat turbulence) or flatter (in the Kolmogorov case) spectral tails with cutoffs in the resonance energy range. By comparison of Figures 4 and 5 one notes that the critical turbulence amplitude allowing for efficient acceleration at parallel shocks is reduced with increasing shock Lorentz factor.

This character of the acceleration processes at ultrarelativistic parallel shocks deviates from that predicted by numerical simulations using the small-angle scattering approximation for modeling of the perturbed magnetic field structure at the shock (Bednarz & Ostrowski 1998; Gallant & Achterberg 1999; Achterberg et al. 2001; Ellison & Double 2004) and confirmed by (semi)analytic approaches (Kirk et al. 2000; Keshet & Waxman 2005), as well as numerical models using other approaches (e.g., Lemoine & Pelletier 2003). All these studies indicate formation of the power-law particle spectrum with the asymptotic ( $\gamma \rightarrow \infty$ ) spectral index  $\alpha \approx 4.2 - 4.3$ . However, as discussed in Ostrowski & Bednarz (2002), these acceleration models do not consider the effects of realistic turbulence at the shock, and in particular the significant role played by the long-wave perturbations. The different character of the acceleration processes at parallel shocks obtained in the present approach is an effect of the downstream magnetic field compression discussed above for oblique superluminal shocks. In the case of large-amplitude perturbations, the compression of tangential magnetic field components leads to the formation of an effectively perpendicular shock configuration. In such conditions, the efficiency of particle acceleration critically depends on the ability of particles to diffuse across field lines of the compressed turbulence. However, as the results for superluminal shocks show, the anisotropic diffusion involved is relatively inefficient for the compressed highly perturbed fields and the final particle spectra become very steep (see the results for  $\delta B/B_{0,1} = 3.0$  and 1.0 in Figure 4 and  $\delta B/B_{0,1} = 3.0, 1.0$  and 0.3 in Figure 5). Note also, that features analogous to the ones observed in superluminal

shocks — dependence of the particle distribution on the shock Lorentz factor, variation of the spectral slope in the case of the Kolmogorov turbulence — appear in the spectra for the parallel shocks. As in Niemiec & Ostrowski (2004), particle spectra calculated for the considered small perturbation amplitudes are non-power-law ones in the full energy range, and the spectral index of the power-law part of the spectrum depends on the wave power spectrum of the magnetic field turbulence. The deviations of the spectra from the power-law character are due to a limited dynamic range of the field perturbations. Because of the lack of long-wave perturbations for high-energy particles with  $k_{res} < k_{min}$ , locally oblique field configurations cannot be formed and particles can be only transmitted downstream of the shock and escape.<sup>8</sup>

The angular distributions for parallel shocks with  $\gamma_1 = 10$  are presented in Figure 6. For mildly perturbed ( $\delta B/B_{0,1} = 1.0$ ) magnetic fields ( $q = 5/3$  – *squares* and  $q = 1$  – *stars*), one can see the features observed in the angular distributions for oblique superluminal shocks (Fig. 3). The differences in the distributions for small-amplitude perturbations ( $\delta B/B_{0,1} = 0.1$ ) reflect the difference in the spectral indices for power-law parts of the particle spectra for the flat (*dashed line*) and Kolmogorov (*solid line*) turbulence.

#### 4. SUMMARY AND DISCUSSION

The results presented here for the first-order Fermi acceleration modeling at ultrarelativistic shock waves reveal several unknown earlier features of such processes. The most important finding of this work is that the generated particle spectra substantially depend on the form of the magnetic turbulence near the shock — contrary to the widely distributed opinion in the present literature. Simulations show a significant role of the perturbed magnetic field compression at the shock, which leads to highly anisotropic particle diffusion conditions in the approximately 2D turbulence formed downstream of the shock. In the case of the flat turbulence spectrum, the continuity of the magnetic field lines across the shock, and a limited particle diffusion along the shock normal in the downstream region result in the formation of very steep spectral tails with cutoffs within the resonance energy range considered. The spectra derived for the Kolmogorov turbulence show, that the existence of high-amplitude long-wave magnetic field perturbations can substantially modify the acceler-

---

<sup>8</sup>Note that in calculations of the spectra for smallest perturbation amplitudes we applied upper energy limits for the accelerated particles (see §2.2;  $E_{max,2} = 3 \cdot 10^3$  and  $E_{max,2} = 10^4$  for  $\gamma_1 = 10$  and  $\delta B/B_{0,1} = 0.1$ , and for the flat and Kolmogorov turbulence, respectively, and  $E_{max,2} = 2 \cdot 10^3$  for  $\gamma_1 = 30$  and  $\delta B/B_{0,1} = 0.05$ ), because simulations of high-energy spectral tails require excessive run times. Therefore, the extension of the spectral cutoffs to high energies was not reliably studied for these few cases.

ation process, allowing for the formation of more extended and flatter spectral components at superluminal shocks, as well as very flat components at parallel shock waves. However, also in this case the spectrum steepening begins and/or the energy cutoff occurs a few orders of magnitude below the maximum particle energy corresponding to the resonance condition for the longest waves upstream of the shock. The simulations also show that for the same background conditions the shock waves with larger Lorentz factors produce steeper spectra with lower cutoff energies.

The compressed magnetic field turbulence structure downstream of the shock is expected to relax with time to the lower-energy isotropic 3D distribution. This may involve various plasma heating and cosmic ray acceleration processes, discussion of which is outside the scope of the present paper. We note, however, that the characteristic time scale for such the isotropization at the given wavelength  $\lambda$  can be estimated as  $\tau_{iso} > \lambda/V_A$  ( $V_A < c$  is the Alfvén velocity in the downstream medium), so that the relaxation processes cannot completely remove the considered anisotropy at the gyration time scale for particles with  $r_g \lesssim \lambda$ . Thus, such particles are always influenced downstream of the shock by the respective resonance and long-wave *anisotropic* structure.

In the following paper (Niemić & Ostrowski, in preparation) we will present a further extension of the present model by including into consideration a highly nonlinear short-wave turbulent component, analogous the one formed at the shock due to plasma instabilities discussed in the literature (see §2.1).

Our present results for ultrarelativistic shock waves, as well as the results obtained for mildly relativistic shocks (Niemić & Ostrowski 2004), require revision of many earlier discussions of cosmic-ray acceleration up to very high energies at relativistic shock waves. The results show, that turbulent conditions near the shock which are consistent with the shock jump conditions can lead to substantial modifications of the acceleration picture with respect to the simplified models producing the wide-range power-law energy distributions, often with the “asymptotic” or “universal” spectral index. With the turbulent magnetic field structures analyzed here, the generation of ultra-high-energy cosmic rays at ultrarelativistic shocks is ineffective. The role of the first-order Fermi process on the observational properties of astrophysical sources hosting relativistic shock waves requires serious reanalysis.

Recently we have become aware of the work by Lemoine & Revenu (2005), who modified the approach of Lemoine & Pelletier (2003) to discuss particle acceleration at high- $\gamma$  shocks with the downstream magnetic field structure obtained from the shock jump conditions. Unfortunately, the numerical method used in both papers does not take into account the correlations between upstream and downstream trajectories at particle shock crossings, which are introduced by the field structure. This is caused by the separate statistical averaging of



the particle transport properties upstream and downstream, and the subsequent treatment of these distributions as independent. Therefore, the method cannot properly reproduce the resulting correlations in particle energy gains, return probabilities, and the respective propagation times at successive shock crossings (e.g., Bednarz & Ostrowski 1996) and their effect on the final particle spectra. The approach is thus unable, or only partially able, to reproduce the results obtained with more realistic background conditions discussed in Niemiec & Ostrowski (2004) and in the present paper.

We are grateful to Martin Pohl for useful discussions of the results and for providing valuable comments and suggestions on the manuscript. We also thank David Carter-Lewis for carefully reading the manuscript. The present work was supported by the Polish State Committee for Scientific Research in 2002-2005 as a research project PBZ-KBN-054/P03/2001, and by MNIł in 2005-2008 as a research project 1 P03D 003 29.

## A. PARTICLE DIFFUSION DOWNSTREAM OF THE SHOCK

In our simulations the magnetic field structure downstream of the shock becomes effectively two-dimensional, perpendicular to the shock normal. Due to the inefficient particle cross-field diffusion, advection of particles with the general downstream flow leads to high particle escape rates resulting in steep particle spectra.

To better understand propagation conditions in this region, we derived particle diffusion coefficients  $\kappa_i$  ( $i = x, y, z$ ) along the three axes in the downstream plasma rest frame, following the method described in Ostrowski (1993) (see also Michałek & Ostrowski 1997). The modeling shows a highly anisotropic diffusion downstream of the shock, with the coefficient along the shock normal  $\kappa_x \ll \kappa_y, \kappa_z$ . For the example considered in Fig. 7 of the shock wave with  $\gamma_1 = 5$ , propagating in the magnetic field with the mean field inclination  $\psi_1 = 45^\circ$  and the flat wave power spectrum of the (upstream) amplitude  $\delta B/B_{0,1} = 3.0$ , the downstream diffusion coefficients for particles of energy  $E = 1$  are  $\kappa_y/\kappa_x \sim 4 \cdot 10^2$  and  $\kappa_z/\kappa_x \sim 3 \cdot 10^2$ . The difference between  $\kappa_y$  and  $\kappa_z$  comes from the contribution of the mean field component which lies in the  $x - y$  plane ( $\psi_2 = 86^\circ$  in this case). The exact values of the diffusion coefficients depend on particle energy. One should note, however, that the diffusion coefficient values derived here can serve only as a general characterization of the propagation properties downstream of the shock. They represent particle motion on time scales much larger than the particle gyration time scale, the latter being important in the modeling of the relativistic shock acceleration.

## REFERENCES

- Achterberg, A., Gallant, Y. A., Kirk, J. G., & Guthmann, A. W. 2001, *MNRAS*, 328, 393
- Ballard, K. R., & Heavens, A. 1992, *MNRAS*, 259, 89
- Bednarz, J., & Ostrowski, M. 1996, *MNRAS*, 283, 447
- Bednarz, J., & Ostrowski, M. 1998, *Phys. Rev. Lett.*, 80, 3911
- Begelman, M. C., & Kirk, J. G. 1990, *ApJ*, 353, 66
- Drury, L. O’C. 1983, *Rep. Prog. Phys.*, 46, 973
- Ellison, D. C., Jones, F. C., & Reynolds, S. P. 1990, *ApJ*, 360, 702
- Ellison, D. C., & Double, G. P. 2004, *Astroparticle Phys.*, 22, 323
- Frederiksen, J. T., Hededal, C., Haugbolle, T., & Nordlund, A. 2004, *ApJ*, 608, L13
- Gallant, Y. A., & Achterberg, A. 1999, *MNRAS*, 305, L6
- Giacalone, J., & Jokipii, J. R. 1994, *ApJ*, 430, L137
- Heavens, A., & Drury, L. O’C. 1988, *MNRAS*, 235, 997
- Jones, F. C., Jokipii, J. R., & Baring, M. G. 1998, *ApJ*, 509, 238
- Keshet, U., & Waxman, E. 2005, *Phys. Rev. Lett.*, 94, 111102
- Kirk, J. G., Guthmann, A. W., Gallant, Y. A., & Achterberg, A. 2000, *ApJ*, 542, 235
- Kirk, J. G., & Duffy, P. 1999, *J. Phys. G*, 25, R163
- Kirk, J. G., & Heavens, A. 1989, *MNRAS*, 239, 995
- Kirk, J. G., & Schneider, P. 1987, *ApJ*, 315, 425
- Lucek, S. G., & Bell, A. R. 2000, *MNRAS*, 314, 65
- Lemoione, M., & Revenu, B. 2005, *MNRAS*, submitted (astro-ph/0510522)
- Lemoione, M., & Pelletier, G. 2003, *ApJ*, 589, L73
- Medvedev, M. V., & Loeb, A. 1999, *ApJ*, 526, 697
- Michalek, G., & Ostrowski, M. 1997, *A&A*, 326, 793

- Naito, T., & Takahara, F. 1995, MNRAS, 275, 1077
- Niemiec, J., & Ostrowski, M. 2004, ApJ, 610, 851
- Niemiec, J. 2005, in AIP Conf. Proc. 801, Astrophysical Sources of High Energy Particles and Radiation, ed. T. Bulik, B. Rudak, & G. Madejski, 385 (astro-ph/0509686)
- Nishikawa, K.-I., Hardee, P., Richardson, G., Preece, R., Sol, H., & Fishman, G. J. 2003, ApJ, 595, 555
- Ostrowski, M. 1991, MNRAS, 249, 551
- Ostrowski, M. 1993, MNRAS, 264, 248
- Ostrowski, M., & Bednarz, J. 2002, A&A, 394, 1141
- Press, W., Teukolsky, S. A., Vetterling, W. T., & Flannery, B. P. 1992, Numerical Recipes in FORTRAN 77 (2d ed.; Cambridge: Cambridge University Press)
- Silva, L. O., Fonseca, R. A., Tonge, J. W., Dawson, J. M., Mori, W. B., & M. Medvedev, M. V. 2003, ApJ, 596, L121
- Webb, G. M., Axford, W. I., & Terasawa, T. 1983, ApJ, 270, 537

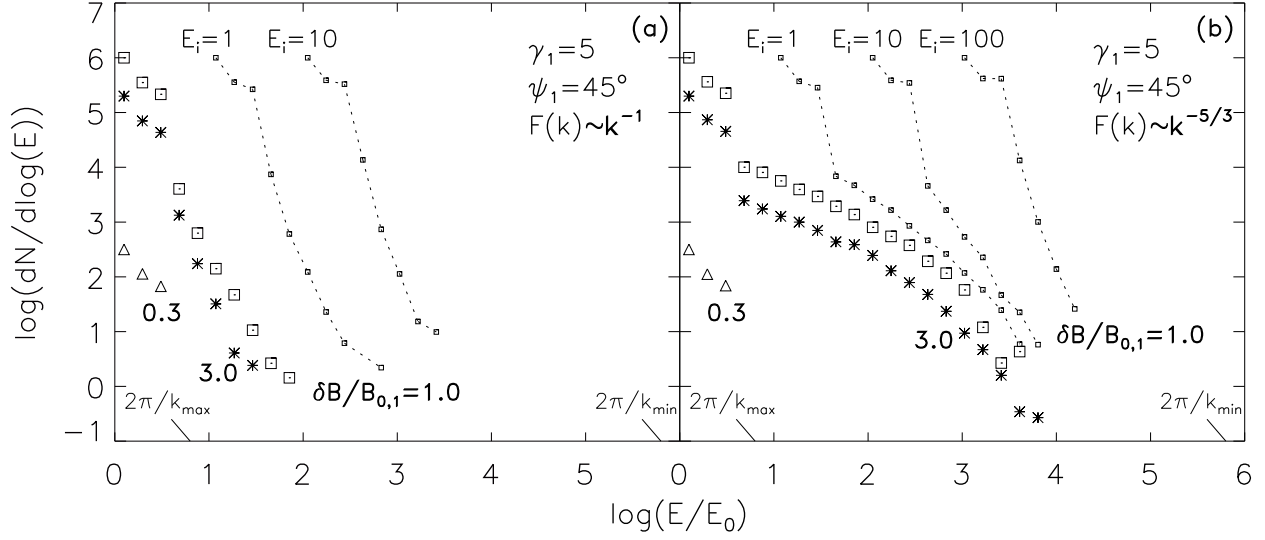


Fig. 1.— Accelerated particle spectra at oblique superluminal shock waves with  $\gamma_1 = 5$  and  $\psi_1 = 45^\circ$  for (a) the flat and (b) the Kolmogorov wave spectrum of magnetic field perturbations. Any individual point in the spectrum represents a particle number ( $\equiv$  weight)  $dN$  recorded per a logarithmic energy bin. The upstream perturbation amplitude  $\delta B/B_{0,1}$  is given near the respective results. The additional spectra obtained for higher injection energies  $E_i = 1, 10$  (and  $100$  in Fig. 1b) are calculated for  $\delta B/B_{0,1} = 1.0$ . Some spectra are vertically shifted for clarity. Particles in the range indicated as  $(2\pi/k_{max}, 2\pi/k_{min})$  can satisfy the resonance condition  $k_{res} = 2\pi/r_g(E)$  for some of the waves in the turbulence spectrum. The particle spectra are measured in the shock normal rest frame.

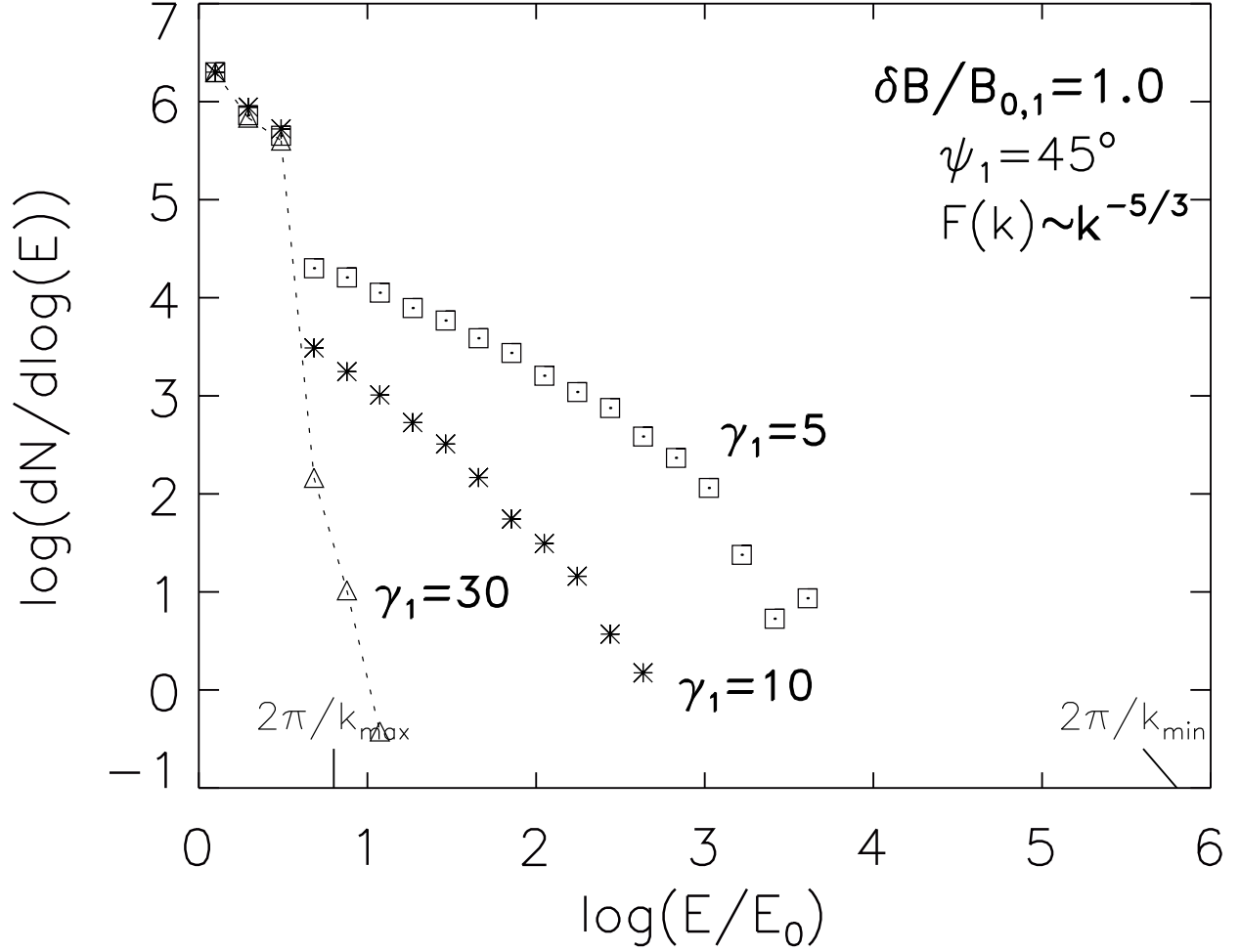


Fig. 2.— Accelerated particle spectra at oblique superluminal shock waves for different shock Lorentz factors  $\gamma_1$ . The results are for the mean field inclination  $\psi_1 = 45^\circ$  and the Kolmogorov wave power spectrum with  $\delta B/B_{0,1} = 1.0$ .

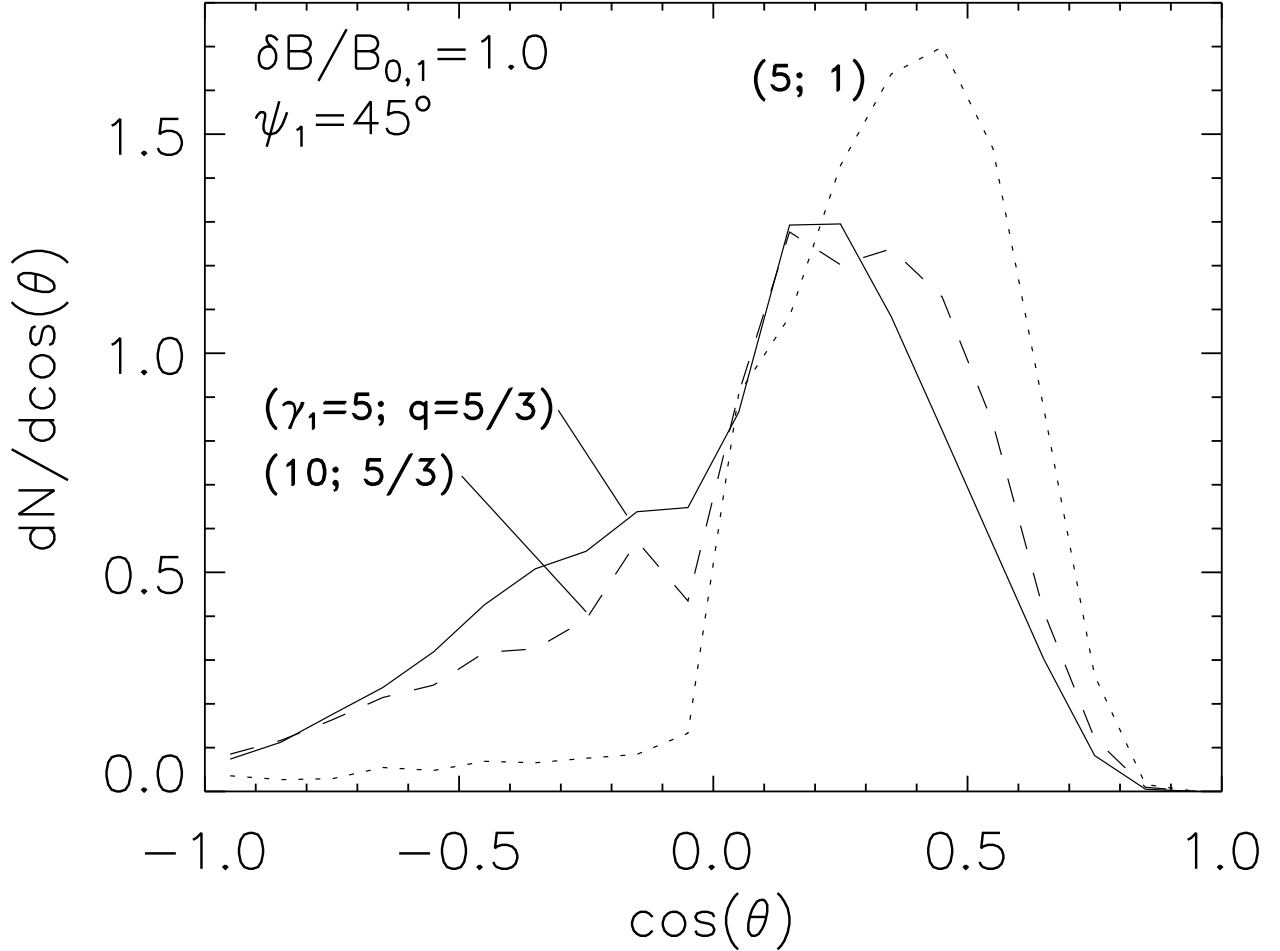


Fig. 3.— Particle angular distributions at the superluminal shock waves for  $\delta B/B_{0,1} = 1.0$  and  $\psi_1 = 45^\circ$ , in the shock rest frame. The curves are calculated by summing the quantity  $w/(|v_x|+0.005)$  in the respective  $\cos\theta$  bins at every particle shock crossing, where  $\theta$  is the angle between the particle momentum and the shock normal,  $v_x$  is a normal component of the particle velocity and  $w$  is its weight. The low-energy particles, with larger weights, thus provide the main contribution to the angular distributions. Only particles forming energetic spectral tails in the energy spectra shown in Fig. 1 are included — the distributions are averaged over particle energies and, therefore, approximate. The angular distributions for the Kolmogorov wave power spectrum ( $q = 5/3$ ) and  $\gamma_1 = 5$  and 10 are presented with the solid and dashed lines, respectively, and for the flat wave power spectrum ( $q = 1$ ) and  $\gamma_1 = 5$  by the dotted line. All distributions are normalized to the unit surface area under the respective curves. Particles with  $\cos\theta < 0$  are directed upstream of the shock.

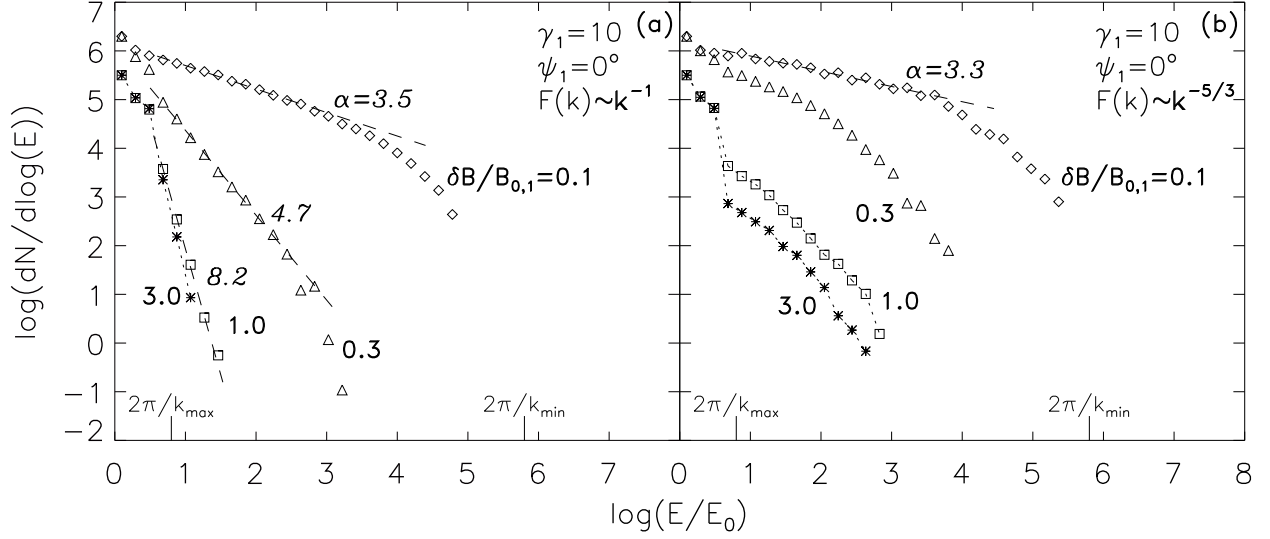


Fig. 4.— Particle spectra at parallel shock waves with  $\gamma_1 = 10$ . The perturbed magnetic field parameters are given in each panel. Linear fits to the power-law parts of some spectra are presented, with the phase-space spectral indices values  $\alpha$  given in italic.

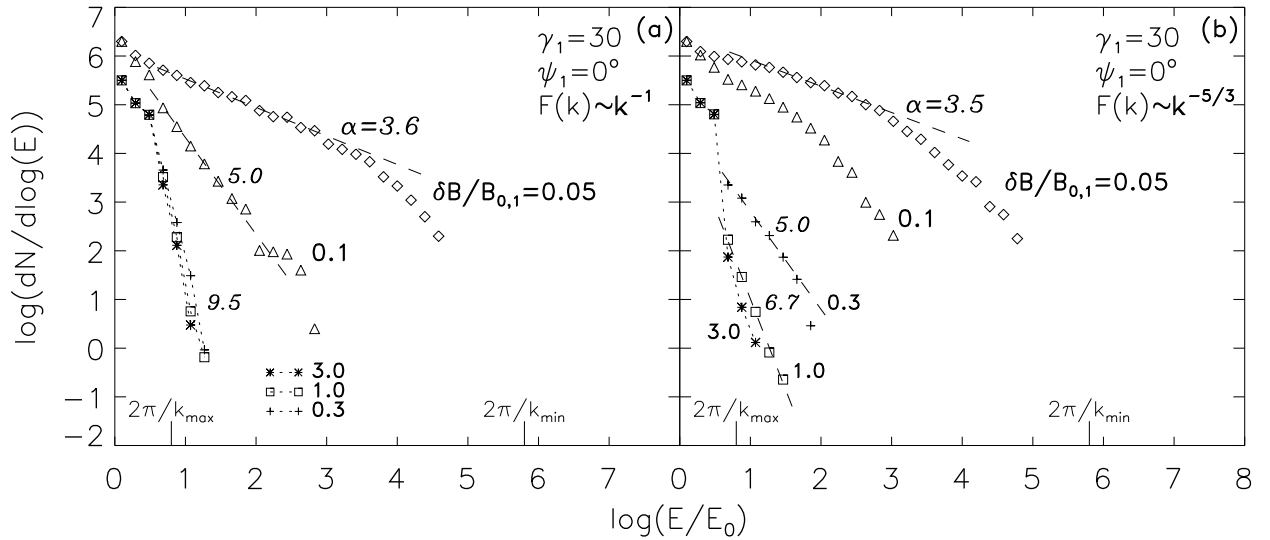


Fig. 5.— Particle spectra at parallel shock waves with  $\gamma_1 = 30$  (see description of Fig. 4).

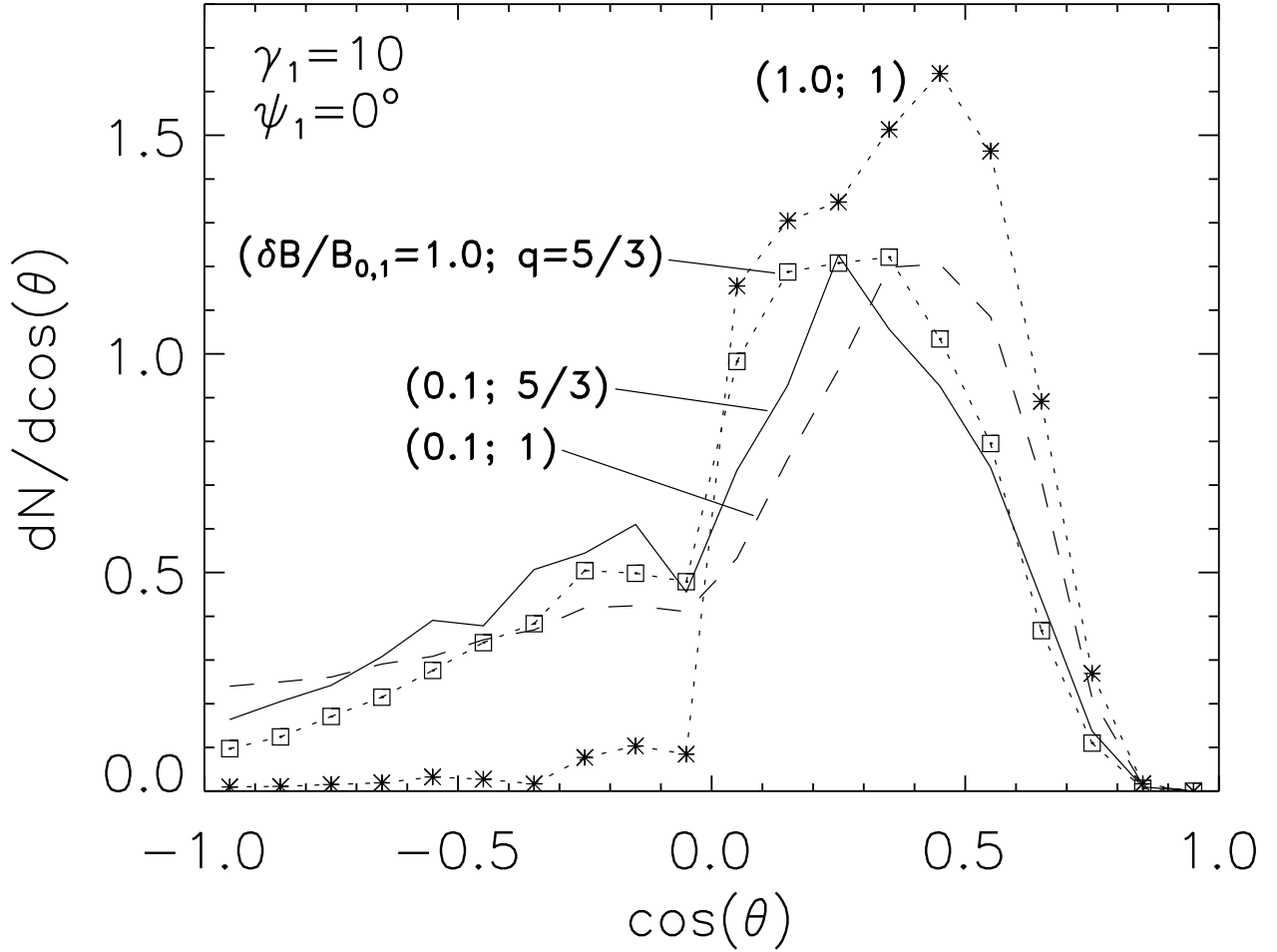


Fig. 6.— Particle angular distributions at parallel shock waves with  $\gamma_1 = 10$ . The distributions for the large turbulence amplitude ( $\delta B/B_{0,1} = 1.0$ ) are for particles forming energetic spectral tails (Fig. 4) and are presented with squares and stars for the Kolmogorov and the flat wave power spectrum, respectively. Angular distributions for the small-amplitude perturbations ( $\delta B/B_{0,1} = 0.1$ ), shown with the solid ( $q = 5/3$ ) and dashed lines ( $q = 1$ ), are formed by particles of energy  $E_s \geq 1$  in the shock rest frame.



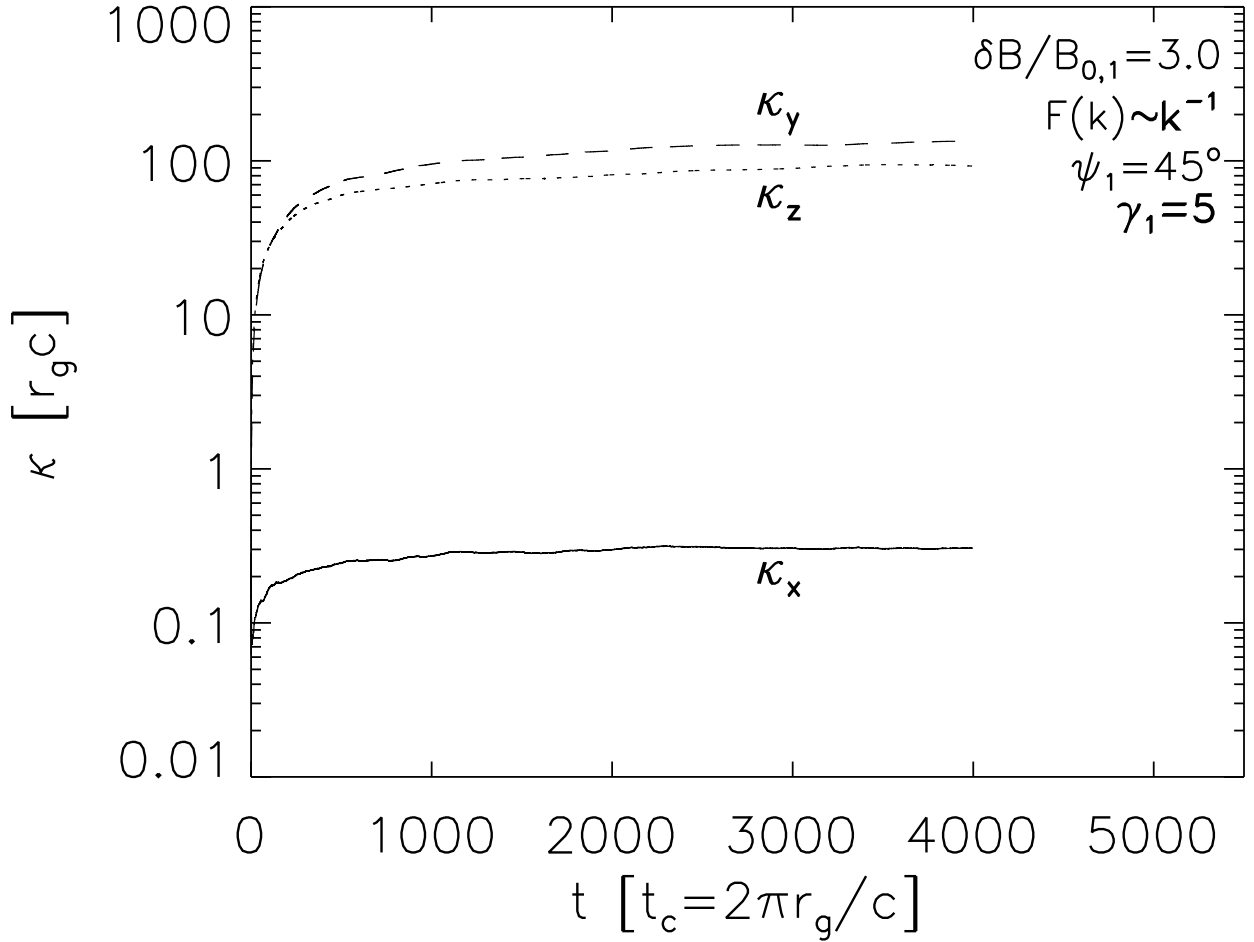


Fig. 7.— Modeling of diffusion coefficients  $\kappa_i$  ( $i = x, y, z$ ) in the compressed perturbed magnetic field downstream of the shock for particles of energy  $E_2 = 1$  and for the shock wave with  $\gamma_1 = 5$ ;  $t$  is the simulation time. The mean field inclination is  $\psi_1 = 45^\circ$  and the amplitude of the turbulent component with the flat power spectrum is  $\delta B / B_{0,1} = 3.0$  upstream of the shock. Particle gyroradius  $r_g$ , applied as a measure of the diffusion coefficient and time unit, is calculated for the average downstream magnetic field.